Quantitative Analysis of Structural Defect in Silicalite by Rietveld Refinements Using X-ray Powder Diffraction and ^{29}Si MAS NMR

Masamichi Inui,[1,2] **Takuji Ikeda,***[1] **Tatsuya Suzuki,**[2] **Keisuke Sugita,**[2] **and Fujio Mizukami**[1]

[1]Research Center for Compact Chemical Process, National Institute of Advanced Industrial Science and Technology, AIST Tohoku, Sendai 983-8551

[2]Sumitomo Chemical Co., Ltd., Basic Chemicals Research Laboratory, 5-1 Sobiraki-cho, Niihama 792-8521

Received March 31, 2009; E-mail: takuji-ikeda@aist.go.jp

The results of conventional powder X-ray diffraction and ^{29}Si solid-state MAS NMR spectroscopy were used to investigate the distribution of Si atom defects in a silicalite optimized for the vapor-phase Beckmann rearrangement process. Powder diffraction data of the dehydrated sample were collected for carrying out accurate Rietveld analysis at room temperature, indicating orthorhombic symmetry of space group *Pnma*. The result of the ^{29}Si MAS NMR spectrum analysis indicated that the number of Si atom defects in silicalite was 1.6 per unit cell. In addition, the result of Rietveld refinement suggested that the defects preferentially appeared at the T2, T3, and T6 sites, which were located along the wall of the straight channels of the MFI structure. The number of lattice defects estimated from the refined structural parameters was 1.5 per unit cell, which was consistent with that estimated from the ^{29}Si MAS NMR analysis.

MFI-type siliceous zeolite silicalite[1] (ideal formula: $Si_{96}O_{192}$) exhibiting hydrophobic property is widely used as a catalyst in various industries. It has two types of channel systems. One system is composed of a straight channel that runs along the [010] direction with 10-membered ring (10-MR) openings of 5.6×5.3 Å^2.[2,3] The other system is composed of a sinusoidal channel that runs along the [100] direction with 10-MR openings of 5.5×5.1 Å^2. The formation of crystal structures with two types of symmetries, namely, orthorhombic *Pnma* and monoclinic $P2_1/n$, has been reported. The former and latter structures comprise 12 and 24 independent Si atom sites, respectively.

It has been elucidated that high-silica zeolite is the most effective catalyst for carrying out the vapor-phase Beckmann rearrangement (VPBR)[4–6] of cyclohexanone oxime to ε-caprolactam. Recently, Sumitomo Chemical Co., Ltd., has successfully carried out the VPBR process using a silicalite catalyst.[7–11] In the VPBR process, silanol nest is indispensable for the catalytic reaction. However, Heitmann et al. reported that some by-products (i.e., cyclohexanone, 2-cyclohexenone, 5-hexenenitrile, etc.) are generated when there is an excess of the silanol group.[12,13] Thus far, the relationship between the catalytic performance of VPBR and the a number of silanol nests in a unit cell has been discussed semiquantitatively by performing FT-IR measurements.[6]

Silanol nest consists of four adjacent silanol groups present at the defect site of a Si atom in a zeolite framework.[14–17] From the results of FT-IR and ^{29}Si MAS NMR measurements, Woolery et al. have reported that two types of internal silanol groups exist in silicalite.[18] One group comprises terminal silanols. The other group has been interpreted to be a hydroxy nest formed due to T-site defects in silicalite.[19–22] Izumi et al. have shown a schematic of a silanol nest which is composed of four hydroxy groups due to deficit of one Si atom from the zeolite framework.[11] In addition, Artioli et al. have shown that the average of the site occupancies of four T-sites an orthorhombic silicalite (T6, T7, T10, and T11, as shown in Figure 1) is 0.75 using a time-of-flight (TOF) neutron powder diffraction.[23] Their sample was prepared by following the procedure described in the Enichem (currently Syndial) patent.[20,24] They also reported that the number of Si atom defects in the framework is eight atoms per unit cell, by carrying out structural analysis of their sample without any modification. This is an interesting report on the periodic distribution of Si atom defects in the MFI crystal. However, the VPBR catalytic performance and local structure information including Si atom defect of their sample were not disclosed in previous works.[19–23] According to the literature, the catalytic performance of the zeolite which increased silanol nests by a post-synthesis (e.g., acid treatment) was not better than that of the zeolite without modification.[12]

From the above results, we consider that the structural properties of silicalite optimized for the VPBR process must be confined to relatively simple as follows. Namely, this means that the existence of a small number of silanol nests is indispensable for demonstrating high catalytic performance. Therefore, Si atom defects in such silicalites must be quantitatively evaluated by carrying out accurate Rietveld refinement and ^{29}Si MAS NMR spectral analysis. In this study, the distribution of silanol nests in a unit cell was investigated using silicalite with a high catalytic performance (i.e., selectivity: >70%).[25]

First, we assume that the number of Si atom defects is in good agreement with the number of silanol nests. Then, the total number of Si atom defects was estimated by performing ^{29}Si MAS NMR measurement. Second, the distribution of Si

Published on the web September 9, 2009; doi:10.1246/bcsj.82.1160

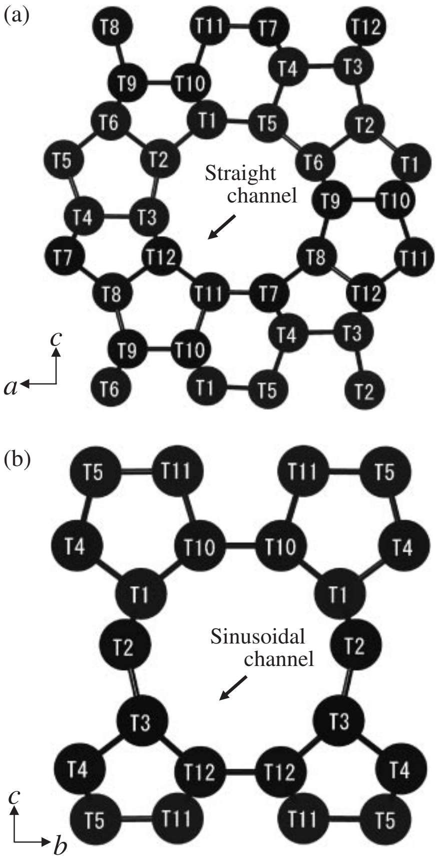

Figure 1. Schematic representation of silicalite orthorhombic phase viewed along (a) the [010] direction and (b) the [100] direction.

atom defects was investigated by the Rietveld analysis. In addition, it was observed that the change in the thermal stability and structural symmetry of our silicalite depended on temperature.

Experimental

Preparation of Silicalite. Silicalite ($Si/Al > 30000$) was synthesized by a hydrothermal method according to the procedure described in the Sumitomo Chemical patent.[25] Fumed silica powder (Japan Aerosil Co., Ltd., 1150 mmol) dispersed in distilled water (33.3 mol) was vigorously mixed with an organic structure directing agent (tetra-*n*-propylammonium bromide: $(C_3H_7)_4NBr$, 182.5 mmol) dissolved in distilled water (6.7 mol) in a 1.5-L autoclave. Then, sodium hydroxide (195 mmol) dissolved in distilled water (2.9 mol) was introduced into the autoclave. The autoclave was heated to and maintained at 463 K for 3 days. After cooling the solution to room temperature, the solid product was filtered, washed with distilled water, dried at 393 K for 16 h, and calcined in flowing air at 773–803 K for 4 h. The obtained product was ion-exchanged with ammonium chloride to remove residual Na^+ ions, washed with distilled water until Cl^- was not detected, dried at 393 K for 16 h, and calcined in flowing air at 773 K for 4 h. The silicalite powder was dehydrated by heating to 400 °C below 7×10^{-4} Pa for 4 h in glass tubes.

Table 1. Experimental Conditions for the High- and Low-Temperature Powder XRD Measurements

Data collection	Temperature range from 7 to 273 K	Temperature range from 376 to 673 K
Instrument	MXP3TA-HRII	D8 ADVANCE Vαrio-1
Geometry	Bragg–Brentano	Debye–Scherrer
Wavelength λ/Å	1.540598 (Cu Kα_1)	1.540598 (Cu Kα_1)
Specimen	Copper flat holder	capillary, 0.7 ϕ (rotation of 60 rpm)
Scan range 2θ/°	23.0–25.0	23.0–25.0
Step size/°	0.016	0.008703
Time per step/s	100	1
Number of steps	125	230

Measurement. A solid-state ^{29}Si dipolar decoupled magic angle spinning nuclear magnetic resonance (DDMAS NMR) spectrum was recorded at a spinning frequency of 4 kHz using a 4 mm MAS probe, a 90° pulse length of 4.7 µs, and a 30 s cycle delay time on a Bruker AMX-500 spectrometer operated at 99.37 MHz. The spectra acquired with 512 scans were accumulated, and the ^{29}Si chemical shifts were calibrated using a standard sample of tetramethylsilane. A solid-state ^1H–^{29}Si cross-polarization magic angle spinning nuclear magnetic resonance (CP/MAS NMR) spectrum was also recorded at a 5 kHz spinning frequency, a contact time of 4 ms, and a 10 s cycle delay time on a Bruker Avance 400 WB spectrometer operated at 79.49 MHz.

Typical characteristic X-ray powder diffraction data of the dehydrated samples was collected at room temperature (293 K) in order to perform the Rietveld analysis using a D8 Advance with a Vαrio-1 diffractometer with a modified Debye–Scherrer geometry and a high-speed 1D position sensitive detector (VÅNTEC-1), under monochromatic Cu Kα_1 radiation. A goniometer was equipped with radial Soller slits to decrease the angular aperture to 2.3°, in order to suppress axial divergence and obtain symmetric profile shapes in low-angle regions.

Crystallographic data have been deposited with FIZ Karlsruhe: Deposition numbers CSD 420746 and CSD 420747. Further details of the crystal structure investigations may be obtained from Fachinformationszentrum Karlsruhe, 76344 Eggenstein-Leopoldshafen, Germany (fax: +49-7247-808-666; e-mail: crysdata@fiz-karlsruhe.de, http://www.fiz-karlsruhe.de/request_for_deposited_data.html) on quoting the appropriate CSD number.

In a high-temperature experiment, the temperature was controlled in the range of 303–683 K by a capillary heater stage (mri, Physikalische Geräte GmbH), which was mounted on the above diffractometer. The rate of increase in temperature was 1 °C min^{-1}. Dehydrated samples were sealed into borosilicate capillary tubes with inner diameters of 0.5 and 0.7 mm for carrying out structural refinement and high-temperature measurement, respectively; these capillary tubes were placed in a glove box filled with purified He gas. The concentrations of oxygen and water molecules in He gas were maintained at less than 1 ppm, in order to prevent readsorption of atmospheric water molecules.

Low-temperature XRD data were collected using a MAC Science MXP3TA-HRII diffractometer with a vertical θ:θ geometry and equipped with a pair of long Soller slits with an angular aperture of 2°. Monochromatic Cu Kα_1 radiation was used. A closed-cycle cryostat (CTI-Cryogenics Model 22) was used to maintain the temperature between 7 and 273 K. The dehydrated samples were packed into a copper holder in order to increase thermal conduction. The goniometer was also equipped with variable-width divergence and scattering slits, in order to improve counting statistics in the high-2θ region at a constant irradiation width of 20 mm. The variable slits also helped in suppressing the

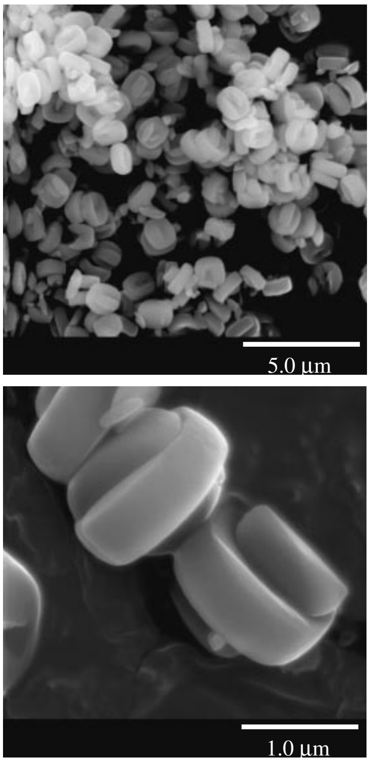

Figure 2. Scanning electron micrographs of silicalite.

background level in the low-2θ region. Throughout the subsequent data analyses, observed intensities were corrected to the fixed-slit data by a model function. Table 1 lists the conditions required for performing high and low XRD measurements on silicalite.

Scanning electron micrographs were obtained using a Hitachi FE-SEM S-800 operated at 15 kV; crystal morphology of the samples was determined from these images. Thermogravimetric analysis was carried out using a Bruker TG-DTA 2020SR at a heating rate of 10 K min^{-1} up to 1373 K under dry airflow conditions.

Results and Discussion

SEM, TG-DTA, and Powder XRD Measurements. As shown in Figure 2, the silicalite crystal has an average length of 1.5 µm. In most crystallites, orthogonally oriented intergrowths are also observed. The thermogravimetry and differential thermal analysis (TG-DTA) curves show a small weight loss of ca. 1.9% and a gradual endothermal peak at 1023 K (Figure 3). The weight loss of ca. 1.0% on sample heating to 500 K is attributed to the dehydration of residual water molecules. Subsequent weight loss with an endothermal peak probably indicates dehydration condensation between the internal silanol groups. In addition, as shown in Figure 4, powder XRD patterns of the samples before and after TG-DTA measurement show a good crystallinity with a narrow peak width. The above results indicate that our silicalite has a high thermal stability and a uniform size and shape; these results indicate that a decrease in crystallinity or a formation of amorphous phases due to structural collapse is hardly recognized by thermal treatment up to 1373 K.

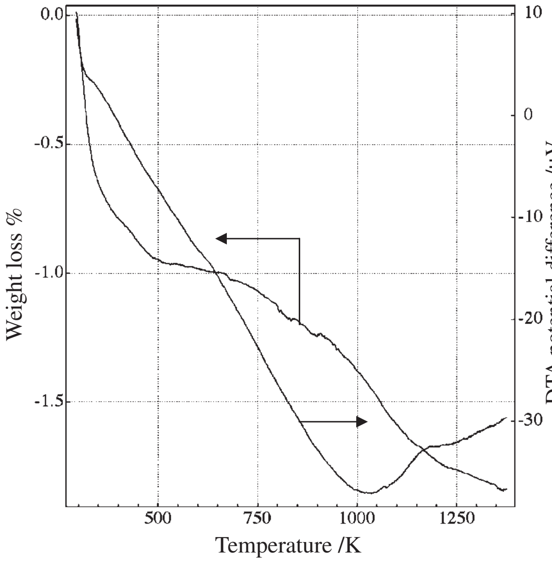

Figure 3. TG-DTA curves of silicalite up to 1373 K.

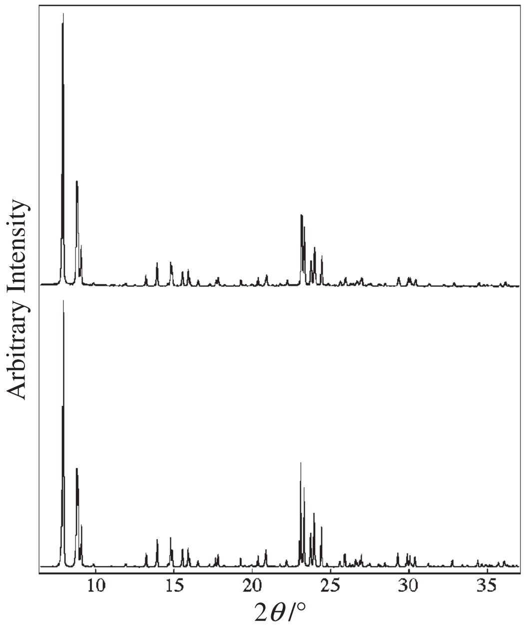

Figure 4. Powder XRD patterns of the sample (a) before and (b) after carrying out thermogravimetric analysis up to 1373 K.

^{29}Si MAS NMR. The number of Si atom defects was estimated from the ^{29}Si DDMAS NMR spectrum. Figure 5 shows the correlation between the Q^3/Q^4 ratio (Q^3: (OSi)$_3$-SiOH, Q^4: Si(OSi)$_4$, Q^3: area of (OSi)$_3$SiOH, Q^4: area of Si(OSi)$_4$) and the number of Si atom defects in the silicalite. Ideal chemical formula of the silicalite is $Si_{96}O_{192}$. The Q^3/Q^4 ratio was calculated from the following equation.

$$Q^3/Q^4 = 4x/(96 - 5x) \qquad (1)$$

where x denotes that the number of Si atom defects. In this equation, the isolated Si atom defects distributed in silicalite were considered; however the contribution of the terminal silanol groups located on the surfaces of the crystal particle was neglected.

Figure 6 shows the ^{29}Si CP/MAS NMR and the ^{29}Si DDMAS NMR spectra of the samples, respectively. From

Table 2. Crystal Size, the Number of the Periodic Lattice on Each Crystal Plane, the Number of Q^3 and Q^4 Structures, and the Estimated Q^3/Q^4 Ratio

		This work	Woolery et al.
Dimension of crystal/µm	*a*-direction	1.5	0.5[a]
	b-direction	0.7	0.23[a]
	c-direction	1.8	0.6[a]
Number of periodic lattices	(100) plane	4.8×10^5	5.4×10^4
	(010) plane	1.0×10^6	1.2×10^5
	(001) plane	2.6×10^5	2.9×10^4
Number of Q^n structures	Q^4	3.5×10^{10}	1.3×10^9
	Q^3	4.9×10^7	5.5×10^6
	Overlapped Q^3 on crystal edge	9.9×10^3	3.3×10^3
	Corrected Q^3	4.9×10^7	5.5×10^6
$Q^3/Q^4 \times 10^2$		0.14	0.43

a) Denotes crystal dimensions from Woolery et al.[16]

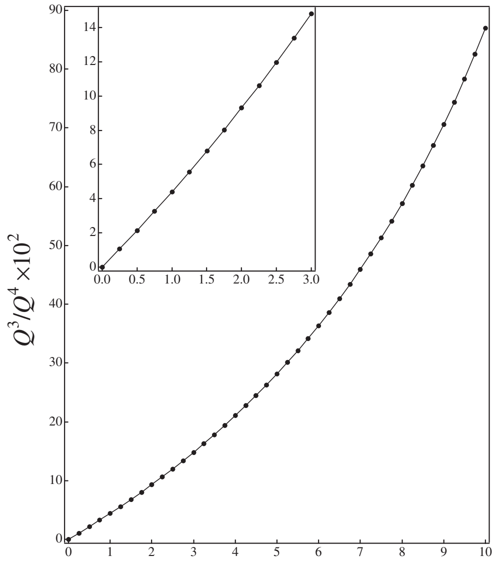

Figure 5. Calculated curves for the relationship between Q^3/Q^4 ratio and the number of Si defects in silicalite using a random isolated vacancy model.

Figures 6a and 6b, it can be observed that the spectral widths were remarkably broad, which suggests that the local symmetry of SiO_4 tetrahedrons was lowered due to structural distortion in the framework. From the ^{29}Si DDMAS NMR spectrum (Figure 6a), the threshold value of the chemical shift value between Q^3 and Q^4 structures was found to be −109.5 ppm. The threshold is clarified in the ^{1}H–^{29}Si CP/MAS NMR spectrum (Figure 6b) by the considerably enhanced Q^3 peaks. From this result, it can be noted that terminal oxygen atoms of the Q^3 sites are protonated and form isolated silanol groups (Si–OH). If eight Si atom defects per unit cell of the silicalite are assumed,[23] the estimated Q^3/Q^4 ratio is more than 50%, as shown in Figure 5. In that case, significant Q^3 peaks will be observed in the ^{29}Si DDMAS NMR spectrum.

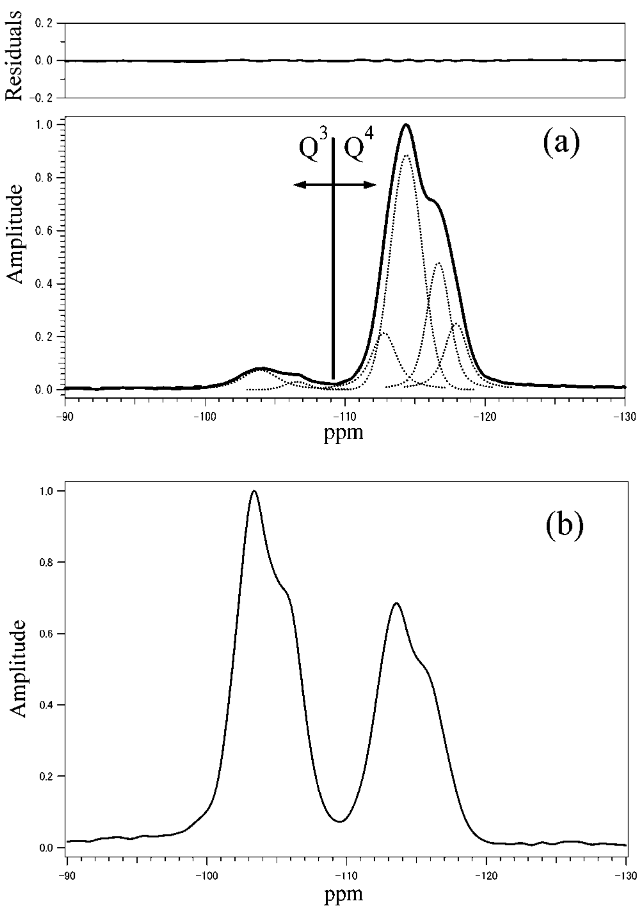

Figure 6. (a) ^{29}Si DDMAS NMR spectrum and (b) ^{29}Si CP/MAS NMR spectrum of silicalite.

On the other hand, small size of the silicalite crystal (<1.0 µm) influences the Q^3/Q^4 ratio because the abundance ratio of terminal silanols derived from the surfaces of crystal particles cannot be disregarded with a decrease in the crystallite size. Table 2 lists the crystallite size, the number of the periodic lattice on each crystal plane, and the number of Q^3 and Q^4 Si atoms. The number of terminal silanol groups on (100), (010), and (001) surface plane are 8, 16, and 16 per unit cell, respectively. A simple approximation of a rectangular crystal shape without internal Si atom defects was adopted for the calculation of the Q^3/Q^4 ratio. From this approximation, the estimated Q^3/Q^4 ratio based on terminal silanols present on the surfaces of crystal particles is ca. 0.1% (Table 2) in our sample, which results in a negligible Q^3/Q^4 ratio. Therefore, the total Q^3/Q^4 ratio is ca. 7.6%, which is estimated from the ^{29}Si DDMAS NMR spectrum by profile fitting with six Gaussian peaks. The individual four Gaussian peaks in the Q^4 region were adopted to estimate the total spectral intensity of Q^4 sites in the curve fitting. Resultantly, the total number of Si atom defects was estimated to be 1.6 per unit cell (1.62 ± 0.06).

We cannot assign these six Gaussian peaks to each T-site in the framework exactly at present, because the spectral resolution of obtained data are too low. It is known that the steam treatment of high-silica ZSM-5 zeolites is effective in the acumination of ^{29}Si DDMAS NMR spectra.[15,17] However, we considered that this sample preparation is not suitable for our study, because Q^3 resonance peaks disappear after the steam treatment as described in Ref. 15. In our preliminary measurement, the disappearance of Q^3 resonances took place by the steam treatment at 200 °C for 48 h (not shown). Probably, some kind of high-resolution 2D ^{29}Si NMR techniques (e.g., COSY or INADEQUATE pulse sequences)[17] will be useful for assignment of each resonance peak.

In the previous study,[18] the Q^3/Q^4 ratio of terminal silanol groups on the surfaces and the total Q^3/Q^4 ratio of silicalite with an average crystallite size of 0.5 µm were ca. 0.4% and ca. 7.5%, respectively. The former Q^3/Q^4 ratio is in good agreement with our estimations listed in Table 2.

Temperature Dependence of Crystal System. The results of low-temperature XRD measurements show that the phase transition between monoclinic and orthorhombic silicalite is below 303 K, as shown in Figure 7. Hay et al. have reported that the phase transition temperature depends on the Si/Al ratio.[26,27] Park et al. have also reported that the phase-transition temperature is approximately 420 K.[28] However, in their studies, the transition temperatures of high silica MFI zeolites are somewhat higher than those of our sample.

Rietveld Refinement. Structure analysis of monoclinic system using low temperature intensity data may indicate a specific defective T-site in 24 T-sites. However, it is easily considered that such an identification of the defective T-site will be difficult by deterioration of the analysis precision derived from increase of the number of refinable structural parameters. Therefore, an orthorhombic system was adopted for the Rietveld refinement of the XRD data at room temperature (293 K), as shown in Figure 8. From the reflection conditions, it was found that the most probable space group of silicalite was *Pnma*. During the structural analysis of silicalite, the Si site occupancy parameters $g(\mathrm{Si})$ were carefully refined in order to estimate the number of defects in our sample (see below). However, estimating $g(\mathrm{Si})$ is a challenge due to the following problems. In general, the occupancy parameters and isotropic atomic displacement parameters determined from the XRD data are strongly correlated. Hence, the parameters of each site cannot be refined simultaneously and independently, because their standard deviations σ are considerably increased. Therefore, the ^{29}Si MAS NMR spectrum provides complementary information, which is indispensable for determining the Si atom defect distribution by carrying out Rietveld refinement.

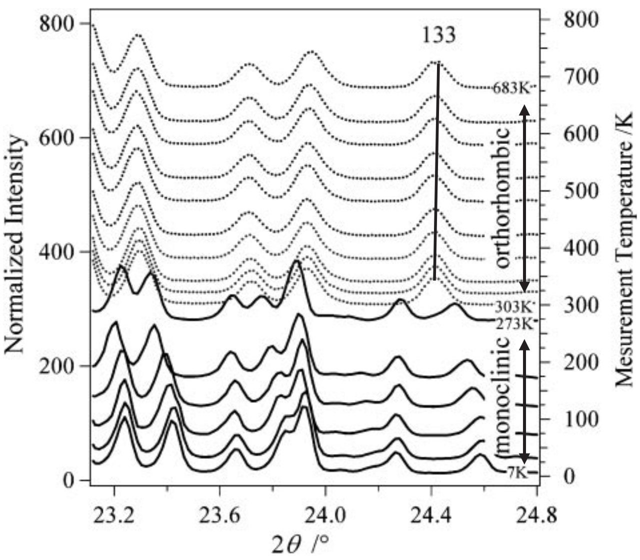

Figure 7. XRD patterns at each temperature from 7 to 683 K.

Rietveld analyses were carried out using the RIETAN-2000 program package.[29] A modified split pseudo-Voigt function was used to model the peak profiles. A composite background function between the 11th-order Legendre polynomial and the preliminary background data are particularly useful for the Debye–Scherrer geometry. The preliminary background data was approximated using the PowderX program.[30] A broad bump around $2\theta = 24°$ observed in the background (Figure 8) was attributed to the capillary tube composed of amorphous borosilicate. In our sample, impurities and amorphous components were rarely observed in XRD patterns that were measured using the Bragg–Brentano geometry, as shown in Figure 4. At the initial stage of the Rietveld analysis, refinement was carried out to impose geometry constraints on the bond lengths $l(\text{Si–O}) = 1.60 \pm 0.01$ Å[31] and bond angles $\phi(\text{Si–O–Si}) = 109.5 \pm 3.0°$. The contribution of the protons of the terminal silanol groups was neglected. In the refinement, the conjugation direction algorithm was applied to nonlinear least-square calculation, whose algorithm makes it possible to escape from local minima easily and automatically. Refined structural models were visualized by means of the program VESTA.[32]

The orthorhombic structure model determined by van Koningsveld et al.[33] was adopted as an initial model for the structural refinement. First, all parameters including $g(\mathrm{Si})$ and $U(\mathrm{Si})$ (isotropic atomic displacement parameter) were refined simultaneously. Since $g(\mathrm{Si})$ and $U(\mathrm{Si})$ are strongly correlated, all $g(\mathrm{Si})$ and $U(\mathrm{Si})$ could not be converged appropriately. Therefore, we adopted two other analytical strategies as follows.

Strategy I: All refinable parameters except $g(\mathrm{Si})$, whose value was fixed to 1.0, were refined. In this strategy, we attempted to identify the defective T-site positions by determining the magnitude relationship among $U(\mathrm{Si})$ values. Refined $U(\mathrm{Si})$ values of sites T2, T3, and T9 were 0.030, 0.030, and 0.033, respectively, which were slightly large, although other $U(\mathrm{Si})$ values were less than 0.03. This suggested that sites T2, T3, and T9 were defective T-sites, although this strategy might be critical evaluation. Table 3 lists the experimental conditions and crystallographic information, while Table 4 lists the structural parameters after refinement.

Strategy II: This strategy was described in a previous

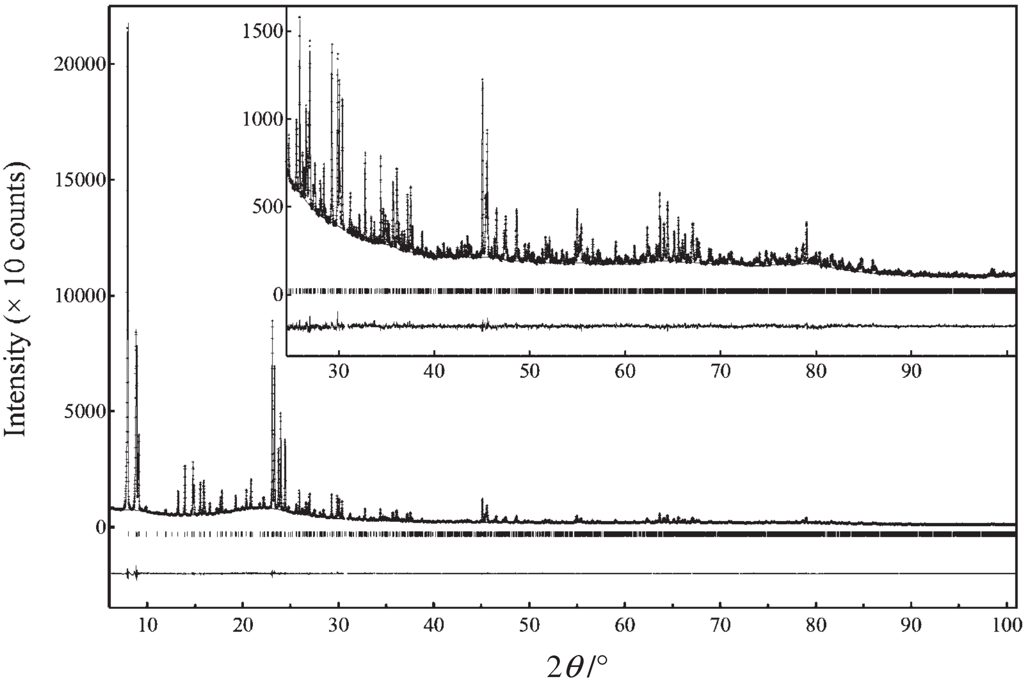

Figure 8. Rietveld refinement patterns of silicalite (293 K). Observed diffraction intensities are represented by a plus (+) sign, and the calculated patterns are represented by a solid line. Curve at the bottom represents the weighted difference, Y_{io}–Y_{ic}, where Y_{io} and Y_{ic} are the observed and calculated intensities of the i-th point, respectively. Short vertical bars below the observed and calculated patterns indicate the positions of the allowed Bragg reflections. Inset shows magnified plots at high 2θ angles.

Table 3. Experimental and Crystallographic Data of Silicalite[a)]

Compound name	Silicalite
Chemical formula	$Si_{96-x}O_{192-4x}(OH)_{4x}$
Space group	*Pnma* (No. 62)
a/Å	20.10160(10)
b/Å	19.90590(12)
c/Å	13.39890(9)
Unit-cell volume/Å^3	5361.44(6)
Wavelength λ/Å	1.540598 (Cu Kα_1)
Specimen	capillary 0.5 ϕ
Rotation speed	60 rpm
2θ range/°	6.0–101.0
Step size/°	0.009073
Profile range in FWHM	16
Number of observations	10471
Number of contributing reflections	2950
Number of structural parameters	117
Number of geometric constrains	120
FWHM/°	0.0675–0.1556
($\Delta d/d$)	(0.01702–0.00235)
Rietveld analysis	
R_{wp}	0.0244
R_P	0.0188
R_e	0.0157
S	1.55
R_B	0.0224
R_F	0.0235

a) Unexpected impurity derived from the capillary glass was excluded from the analysis range.

report by Artioli et al.[23] Isotropic atomic displacement parameters of all the Si and O sites were constrained to be equal in all elements. A two-step refinement process was carried out as follows. (i) Occupancy parameters of all the T-sites g(Si) were fixed to 1.0. Other parameters, including the peak shift, profile, background, atomic coordinates, and lattice parameters, were refined simultaneously. (ii) All the occupancy parameters were refined. If the g(Si) value of any T-site converged and was greater than 1.0, its g(Si) was fixed to 1.0. The iteration between (i) and (ii) was repeated until all g(Si) values converged to less than 1.0 and R-factors did not decrease. (iii) If the number of Si atom defects calculated from the refined g(Si) values was considerably overestimated by referring to the ^{29}Si MAS NMR result, the next analytical step returned to (i).

As a result, both refinements on the basis of the two strategies indicate almost the same defective T-site position. Since sites T2 and T3 are likely to be defective T-sites, we henceforth discuss the refinement of the structural model on the basis of Strategy II. Table 5 lists the refined structural parameters. Figure 8 shows the plot of the observed, calculated, and difference patterns against 2θ after refinement. Finally, the obtained R-factors were found to be sufficiently low.

The Si atom defects were found to be located at the T1, T2, T3, T6, and T9 sites, within standard deviations of g(Si). The total number of Si atom defects was 1.52 ± 0.17, which is consistent with those estimated from the ^{29}Si MAS NMR results. The refined g(Si) values of each site were generally over or underestimated by the analytical error due to the existence of numerous refinable structural parameters (117 parameters), although the numbers of distinguishable peaks and

Table 4. Refined Structural Parameters, g, x, y, z, and $U/\text{Å}^2$ of Silicalite according to Analytical Strategy I[a)]

	M	g	M^*g	x	y	z	U
Si1	8	1	8	0.4228(4)	0.0580(6)	−0.3360(6)	0.028(2)
Si2	8	1	8	0.3091(5)	0.0292(3)	−0.1868(5)	0.030(2)
Si3	8	1	8	0.2794(3)	0.0628(4)	0.0334(5)	0.030(2)
Si4	8	1	8	0.1215(3)	0.0640(4)	0.0288(5)	0.021(2)
Si5	8	1	8	0.0716(4)	0.0283(3)	−0.1825(6)	0.026(3)
Si6	8	1	8	0.1876(4)	0.0579(5)	−0.3262(5)	0.025(2)
Si7	8	1	8	0.4235(4)	−0.1716(4)	−0.3226(7)	0.024(3)
Si8	8	1	8	0.3089(4)	−0.1295(3)	−0.1821(5)	0.019(2)
Si9	8	1	8	0.2734(4)	−0.1723(4)	0.0321(6)	0.033(3)
Si10	8	1	8	0.1189(4)	−0.1740(4)	0.0301(6)	0.022(2)
Si11	8	1	8	0.0708(4)	−0.1294(4)	−0.1826(6)	0.021(2)
Si12	8	1	8	0.1887(5)	−0.1726(3)	−0.3157(6)	0.029(2)
O1	8	1	8	0.3730(7)	0.0536(11)	−0.2450(8)	0.0474(6)
O2	8	1	8	0.3080(7)	0.0558(7)	−0.0759(8)	$=U$(O1)
O3	8	1	8	0.1998(6)	0.0622(6)	0.0290(6)	$=U$(O1)
O4	8	1	8	0.0958(5)	0.0628(7)	−0.0827(9)	$=U$(O1)
O5	8	1	8	0.1164(7)	0.0503(10)	−0.2737(8)	$=U$(O1)
O6	8	1	8	0.2443(6)	0.0550(11)	−0.2443(8)	$=U$(O1)
O7	8	1	8	0.3743(7)	−0.1578(8)	−0.2323(10)	$=U$(O1)
O8	8	1	8	0.3085(8)	−0.1564(6)	−0.0714(9)	$=U$(O1)
O9	8	1	8	0.1959(7)	−0.1537(4)	0.0265(6)	$=U$(O1)
O10	8	1	8	0.0901(6)	−0.1601(6)	−0.0780(10)	$=U$(O1)
O11	8	1	8	0.1195(8)	−0.1560(7)	−0.2660(9)	$=U$(O1)
O12	8	1	8	0.2437(7)	−0.1550(8)	−0.2359(10)	$=U$(O1)
O13	8	1	8	0.3110(6)	−0.0503(7)	−0.1829(6)	$=U$(O1)
O14	8	1	8	0.0791(5)	−0.0508(8)	−0.1728(7)	$=U$(O1)
O15	8	1	8	0.4176(7)	0.1278(7)	−0.3916(10)	$=U$(O1)
O16	8	1	8	0.4052(7)	−0.0020(7)	−0.4093(10)	$=U$(O1)
O17	8	1	8	0.4015(7)	−0.1330(6)	−0.4217(11)	$=U$(O1)
O18	8	1	8	0.1944(10)	0.1284(6)	−0.3825(8)	$=U$(O1)
O19	8	1	8	0.1941(10)	−0.0003(6)	−0.4058(8)	$=U$(O1)
O20	8	1	8	0.1996(9)	−0.1318(6)	−0.4153(8)	$=U$(O1)
O21	8	1	8	−0.0030(7)	0.0481(9)	−0.2048(8)	$=U$(O1)
O22	8	1	8	−0.0035(7)	−0.1488(8)	−0.2082(8)	$=U$(O1)
O23	4	1	4	0.4241(9)	−1/4	−0.3420(11)	$=U$(O1)
O24	4	1	4	0.1916(12)	−1/4	−0.3407(10)	$=U$(O1)
O25	4	1	4	0.2821(8)	−1/4	0.0596(12)	$=U$(O1)
O26	4	1	4	0.1079(10)	−1/4	0.0651(14)	$=U$(O1)

a) M is the multiplicity. Estimated standard deviations are given as uncertainties in the last reported decimal digit.

observed data points were 590 and 10471, respectively, in the XRD pattern. However, the total number of Si atom defects after several analytical cycles converged to almost that same value: ca. 1.5 per unit cell. In addition, the most probable Si atom defect sites were estimated to be T2, T3, and T6, within 3σ of the refined g(Si) values (Table 5).

All the Si atom defect sites were parallel to both the straight channel and the sinusoidal channel of the MFI structure, as shown in Figure 9a. For comparison, Figure 9b also shows the positions of the Si atom defects, as reported by Artioli et al.[23] However, the presence of a Si atom defect at site T10 parallel to the sinusoidal channel could not be observed in our sample. The positional relationship between three defective T-sites forms a one-dimensional chain along the (001) direction, as shown in Figure 10, where the defective T-sites are located on a layer-like building unit composed of 5-MRs. Tables 6 and 7 list the bond lengths l(Si–O) and bond angles ϕ(Si–O–Si) in silicalite calculated from the refined lattice and structural parameters, respectively. The calculated l(Si–O) values range from 1.58 to 1.60 Å; however, the average bond length $l(\text{Si–O}) = 1.585$ Å is somewhat shorter than that estimated in the previous study.[23] These results suggest that the framework of silicalite is stabilized by a strong covalent bond, leading high thermal stability up to 1373 K.

From the above results, it can be concluded that silicalite prepared for VPBR has a very small number of Si atom defects: ca. 1–2 atoms per unit cell; these defects are located along the straight channel and cause silanol nests to be active sites. This result is consistent with the dependence of VPBR catalytic performance on the number of silanol groups estimated in previous studies.[12,13] The distribution and number of Si atom defects observed in our sample were almost different to those reported by Artioli et al., which strongly depend on the synthesis and preparation conditions of silicalite.

Table 5. Refined Structural Parameters, g, x, y, z, and $U/\text{Å}^2$ of Silicalite according to Analytical Strategy II[a)]

	M	g	$M*g$	x	y	z	U
Si1	8	0.993(10)	7.95(8)	0.4228(3)	0.0575(5)	−0.3358(5)	0.0247(4)
Si2	8	0.946(9)	7.57(8)	0.3091(5)	0.0293(3)	−0.1869(5)	=U(Si1)
Si3	8	0.933(9)	7.47(7)	0.2795(3)	0.0627(4)	0.0334(5)	=U(Si1)
Si4	8	1	8	0.1219(3)	0.0636(4)	0.0288(5)	=U(Si1)
Si5	8	1	8	0.0718(4)	0.0287(3)	−0.1825(6)	=U(Si1)
Si6	8	0.964(9)	7.71(7)	0.1879(4)	0.0580(4)	−0.3261(5)	=U(Si1)
Si7	8	1	8	0.4236(4)	−0.1718(4)	−0.3231(6)	=U(Si1)
Si8	8	1	8	0.3092(5)	−0.1293(3)	−0.1814(5)	=U(Si1)
Si9	8	0.973(10)	7.79(8)	0.2737(3)	−0.1726(3)	0.0327(6)	=U(Si1)
Si10	8	1	8	0.1193(4)	−0.1740(4)	0.0302(6)	=U(Si1)
Si11	8	1	8	0.0711(4)	−0.1293(4)	−0.1825(6)	=U(Si1)
Si12	8	1	8	0.1891(5)	−0.1721(3)	−0.3158(5)	=U(Si1)
O1	8	1	8	0.3732(7)	0.0539(11)	−0.2446(9)	0.0501(7)
O2	8	1	8	0.3086(7)	0.0556(7)	−0.0757(8)	=U(O1)
O3	8	1	8	0.2004(6)	0.0615(6)	0.0289(6)	=U(O1)
O4	8	1	8	0.0956(5)	0.0630(7)	−0.0824(9)	=U(O1)
O5	8	1	8	0.1166(7)	0.0500(10)	−0.2744(9)	=U(O1)
O6	8	1	8	0.2446(6)	0.0545(11)	−0.2439(8)	=U(O1)
O7	8	1	8	0.3744(7)	−0.1581(8)	−0.2316(10)	=U(O1)
O8	8	1	8	0.3080(8)	−0.1566(5)	−0.0707(9)	=U(O1)
O9	8	1	8	0.1963(7)	−0.1540(4)	0.0265(6)	=U(O1)
O10	8	1	8	0.0903(6)	−0.1603(6)	−0.0778(11)	=U(O1)
O11	8	1	8	0.1196(7)	−0.1562(7)	−0.2662(9)	=U(O1)
O12	8	1	8	0.2439(7)	−0.1544(8)	−0.2355(10)	=U(O1)
O13	8	1	8	0.3103(6)	−0.0500(8)	−0.1833(6)	=U(O1)
O14	8	1	8	0.0789(5)	−0.0506(8)	−0.1720(7)	=U(O1)
O15	8	1	8	0.4179(7)	0.1279(7)	−0.3917(10)	=U(O1)
O16	8	1	8	0.4059(7)	−0.0017(7)	−0.4102(10)	=U(O1)
O17	8	1	8	0.4012(7)	−0.1323(6)	−0.4214(11)	=U(O1)
O18	8	1	8	0.1949(10)	0.1277(7)	−0.3822(8)	=U(O1)
O19	8	1	8	0.1938(10)	−0.0003(6)	−0.4055(8)	=U(O1)
O20	8	1	8	0.1999(9)	−0.1310(6)	−0.4153(8)	=U(O1)
O21	8	1	8	−0.0031(7)	0.0480(9)	−0.2055(8)	=U(O1)
O22	8	1	8	−0.0031(7)	−0.1489(8)	−0.2084(8)	=U(O1)
O23	4	1	4	0.4245(9)	−1/4	−0.3435(11)	=U(O1)
O24	4	1	4	0.1922(12)	−1/4	−0.3398(10)	=U(O1)
O25	4	1	4	0.2825(8)	−1/4	0.0580(11)	=U(O1)
O26	4	1	4	0.1080(10)	−1/4	0.0648(13)	=U(O1)

a) M is the multiplicity. Estimated standard deviations are given as uncertainties in the last reported decimal digit.

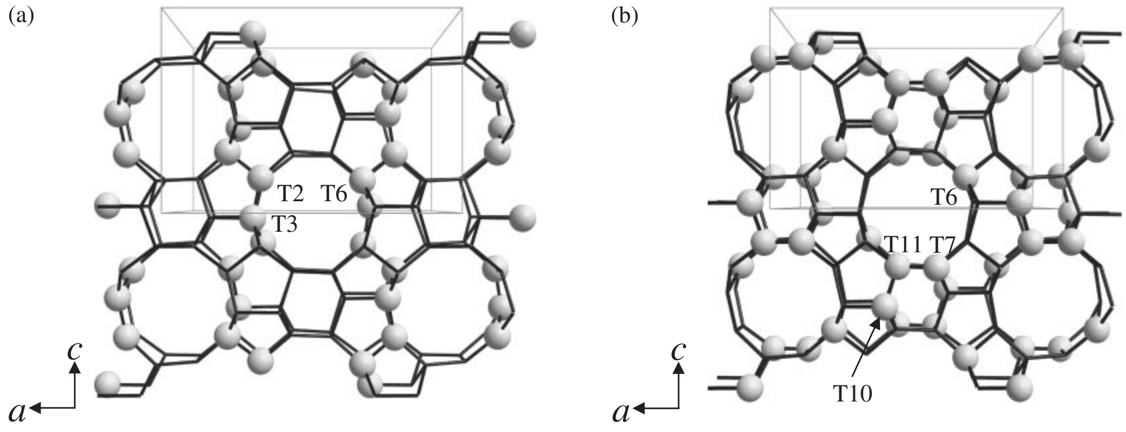

Figure 9. Ball and stick representation of the silicalite orthorhombic structure viewed along the b-direction, including defect Si sites observed for (a) this study and (b) previous study.[17] Large balls (white) show the defective T sites.

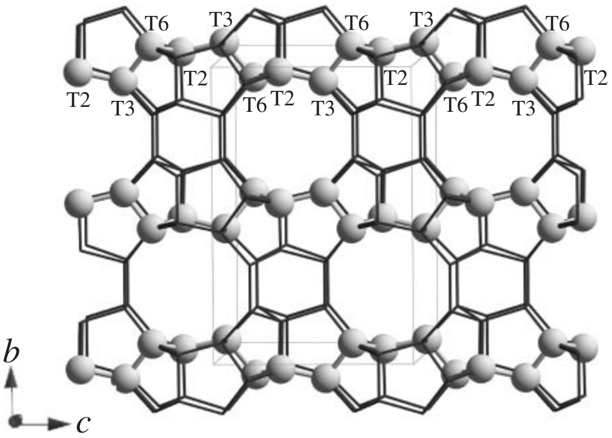

Figure 10. Schematic drawing of the silicalite framework viewed along the (010) direction. Large balls (white) show the defective T sites.

Table 6. Bond Lengths, l/Å, in Silicalite Calculated from the Refined Lattice and Structural Parameters

l(T–O)	Min. l(T–O)	Max. l(T–O)
Si1–O	1.580(14)	1.600(13)
Si2–O	1.580(11)	1.586(14)
Si3–O	1.580(11)	1.591(13)
Si4–O	1.580(11)	1.593(14)
Si5–O	1.580(13)	1.59(2)
Si6–O	1.580(14)	1.600(13)
Si7–O	1.580(7)	1.60(2)
Si8–O	1.580(12)	1.58(2)
Si9–O	1.580(14)	1.600(14)
Si10–O	1.580(14)	1.600(14)
Si11–O	1.580(14)	1.58(2)
Si12–O	1.580(12)	1.585(6)

Conclusion

The long-range ordering of Si atom defects in silicalite prepared for VPBR was crystallographically investigated by the combination of conventional X-ray powder diffraction and solid-state ^{29}Si MAS NMR spectroscopy. The phase transition from monoclinic to orthorhombic was observed at 303 K in our silicalite. The most probable Si atom defect sites were estimated to be T2, T3, and T6 by carrying out Rietveld structural refinement using an orthorhombic model. The total number of Si atom defects estimated by ^{29}Si MAS NMR analysis was 1.6 ± 0.1 per unit cell, which was in good agreement with the value 1.5 ± 0.2 per unit cell estimated from the result of Rietveld refinement. All Si atom defect sites were distributed along the straight channel of the MFI structure in our sample. The position of Si atom defects (sites T2, T3, and T6) determined by the Rietveld analysis might be slightly suspicious due to critical evaluation of g(Si) values. However, the existence of a very small number of Si atom defects and its long-range ordering were confirmed in our silicalite. These defect positions are consistent with the silanol nest (as an active site) distribution neighboring the straight channel opening estimated by a quantum mechanical calculation in previous works.[11]

Table 7. Bond Angles, ϕ/°, in Silicalite Calculated from the Refined Lattice and Structural Parameters

T–O–T	ϕ/°
Si1–O1–Si2	155.2(13)
Si2–O2–Si3	154.7(11)
Si3–O3–Si4	176.9(8)
Si4–O4–Si5	154.8(11)
Si5–O5–Si6	150.8(10)
Si2–O6–Si6	159.3(13)
Si7–O7–Si8	154.3(10)
Si8–O8–Si9	154.0(11)
Si9–O9–Si10	151.8(7)
Si10–O10–Si11	165.5(9)
Si11–O11–Si12	155.9(10)
Si8–O12–Si12	164.2(10)
Si2–O13–Si8	178.1(9)
Si5–O14–Si11	165.1(8)
Si1–O15–Si10	148.4(10)
Si1–O16–Si4	169.6(11)
Si4–O17–Si7	148.3(10)
Si6–O18–Si9	150.7(11)
Si3–O19–Si6	162.2(13)
Si3–O20–Si12	148.1(9)
Si1–O21–Si5	147.8(9)
Si7–O22–Si11	151.9(9)
Si7–O23–Si7	160.0(14)
Si12–O24–Si12	156.1(11)
Si9–O25–Si9	152.1(13)
Si10–O26–Si10	142.3(2)
Min. ϕ(T–O–T)/°	142.3(2)
Max. ϕ(T–O–T)/°	178.1(9)

References

1 E. M. Flanigen, J. M. Bennett, R. W. Grose, J. P. Cohen, R. L. Patton, R. M. Kirchner, J. V. Smith, *Nature* **1978**, *271*, 512.

2 G. T. Kokotailo, S. L. Lawton, D. H. Olson, W. M. Meier, *Nature* **1978**, *272*, 437.

3 D. H. Olson, G. T. Kokotailo, S. L. Lawton, W. M. Meier, *J. Phys. Chem.* **1981**, *85*, 2238.

4 H. Sato, N. Ishii, K. Hirose, S. Nakamura, *Stud. Surf. Sci. Catal.* **1986**, *28*, 755.

5 H. Sato, N. Ishii, K. Hirose, S. Nakamura, Proceedings of the Seventh International Zeolite Conference, **1986**, p. 755.

6 G. P. Heitmann, G. Dahlholl, W. F. Hölderich, *J. Catal.* **1999**, *186*, 12.

7 M. Ishida, T. Suzuki, H. Ichihashi, A. Shiga, *Catal. Today* **2003**, *87*, 187.

8 M. Kitamura, H. Ichihashi, *Stud. Surf. Sci. Catal.* **1994**, *90*, 67.

9 B. Kraushaar, J. W. De Haan, J. H. C. Van Hooff, *J. Catal.* **1988**, *109*, 470.

10 H. Sato, K. Hirose, M. Kitamura, *Nippon Kagaku Kaishi* **1989**, *3*, 548.

11 Y. Izumi, H. Ichihashi, Y. Shimazu, M. Kitamura, H. Sato, *Bull. Chem. Soc. Jpn.* **2007**, *80*, 1280.

12 G. P. Heitmann, G. Dahlhoff, W. F. Hölderich, *Appl. Catal., A* **1999**, *185*, 99.

13 H. Ichihashi, M. Kitamura, *Catal. Today* **2002**, *73*, 23.

14 R. M. Dessau, K. D. Schmitt, G. T. Kerr, G. L. Woolery,

L. B. Alemany, *J. Catal.* **1988**, *109*, 472.

15 R. M. Dessau, K. D. Schmitt, G. T. Kerr, G. L. Woolery, L. B. Alemany, *J. Catal.* **1987**, *104*, 484.

16 R. M. Dessau, K. D. Schmitt, G. T. Kerr, G. L. Woolery, L. B. Alemany, *J. Catal.* **1988**, *109*, 472.

17 C. A. Fyfe, H. Grondey, Y. Feng, G. T. Kokotailo, *J. Am. Chem. Soc.* **1990**, *112*, 8812.

18 G. L. Woolery, L. B. Alemany, R. M. Dessau, A. W. Chester, *Zeolites* **1986**, *6*, 14.

19 V. Bolis, C. Busco, S. Bordiga, P. Ugliengo, C. Lamberti, A. Zecchina, *Appl. Surf. Sci.* **2002**, *196*, 56.

20 A. Zecchina, S. Bordiga, G. Spoto, L. Marchese, G. Petrini, G. Leofanti, M. Padovan, *J. Phys. Chem.* **1992**, *96*, 4985.

21 A. Zecchina, S. Bordiga, G. Spoto, L. Marchese, G. Petrini, G. Leofanti, M. Padovan, *J. Phys. Chem.* **1992**, *96*, 4991.

22 A. Zecchina, S. Bordiga, G. Spoto, D. Scarano, G. Petrini, G. Leofanti, M. Padovan, C. O. Arean, *J. Chem. Soc., Faraday Trans.* **1992**, *88*, 2959.

23 G. Artioli, C. Lamberti, G. L. Marra, *Acta Crystallogr., Sect. B* **2000**, *56*, 2.

24 M. Taramasso, G. Perego, B. Notari, U.S. Patent 4,410,501, **1983**.

25 H. Sato, K. Hirose, N. Ishii, Y. Umada, U.S. Patent, 4,709,024, **1986**.

26 D. G. Hay, H. Jaeger, G. W. West, *J. Phys. Chem.* **1985**, *89*, 1070.

27 D. G. Hay, H. Jaeger, *J. Chem. Soc., Chem. Commun.* **1984**, 1433.

28 S. H. Park, R.-W. Große-Kunstleve, H. Graetsch, H. Gies, *Stud. Surf. Sci. Catal.* **1997**, *105*, 1989.

29 F. Izumi, T. Ikeda, *Mater. Sci. Forum* **2000**, *321–324*, 198.

30 C. Dong, *J. Appl. Cryst.* **1999**, *32*, 838.

31 G. Bergerhoff, K. Brandenburg, in *International Table for X-ray Crystallography*, 3rd ed., ed. by E. Prince, Kluwer Academic Publishers, Dordrecht, **2004**, Vol. C, Chap. 9.4.

32 K. Momma, F. Izumi, *J. Appl. Cryst.* **2008**, *41*, 653.

33 H. van Koningsveld, H. van Bekkum, J. C. Jansen, *Acta Crystallogr., Sect. B* **1987**, *43*, 127.